Nanoscale Horizons

ROYAL SOCIETY OF CHEMISTRY

COMMUNICATION

View Article Online
View Journal | View Issue

Cite this: *Nanoscale Horiz.*, 2021, 6, 341

Received 3rd February 2021,
Accepted 15th February 2021

DOI: 10.1039/d1nh00073j

rsc.li/nanoscale-horizons

Ultratough and ultrastrong graphene oxide hybrid films *via* a polycationitrile approach†

Jian Chang,[a] Miao Zhang,*[a] Qiang Zhao,[b] Liangti Qu*[c] and Jiayin Yuan*[a]

Graphene oxide (GO) is a classic two dimensional (2D) building block that can be used to develop high-performance materials for numerous applications, particularly in the energy and environmental fields. Currently, the precise assembly of GO nanosheets into macroscopic nanohybrids of superior strength and toughness is desirable, and faces challenges and trade-offs. Herein, we exploited the freshly established polycationitrile method as a powerful molecular crosslinking strategy to engineer ultratough and ultrastrong GO/polymer hybrid films, in which a covalent triazine-based network was constructed in a mild condition to reinforce the interface between GO nanosheets. The tensile strength and toughness reached 585 ± 25 MPa and 14.93 ± 1.09 MJ m^{-3}, respectively, which, to the best of our knowledge, are the current world records in all GO-based hybrid films. As an added merit of the tailor-made polymer crosslinker, the high mechanical performance can be maintained in large part at an extremely high relative humidity of 98%. This emerging interface-engineering approach paves a new avenue to produce integrated strong-and-tough 2D nanohybrid materials that are useful in aerospace, artificial muscle, energy harvesting, tissue engineering and more.

New concepts

Graphene oxide (GO) is a classic example of a two-dimensional (2D) material, and one of its key properties of interest is the mechanical behavior. The aim of this study was to advance the mechanical performance of graphene oxide-based hybrid films to a new level by a tailor-made polymer crosslinker termed "polycationitrile" that carries a unique functionality sequence in its repeating unit. The common supramolecular interactions, such as hydrogen bonding, π–π and cation–π interactions, were used to associate the polycationitrile to the GO nanosheets. A unique polytriazine network was then introduced *via* a base-catalyzed, room-temperature cyclization reaction of the nitrile groups that critically improves simultaneously both the tensile strength and toughness. The effectiveness and simplicity in applying polycationitrile chemistry in engineering polymer–inorganic interfaces makes them valuable for construction of high-performance functional 2D materials.

Introduction

Nature provides tailor-made materials, such as nacre, bone, and wood, whose distinct mechanical properties, *e.g.* high stiffness, strength and toughness, stem from their intrinsic building blocks joined exquisitely by interfacial forces at multiple length scales.[1] Inspiration from the wisdom of nature has boosted scientific enthusiasm and passion in assembling two-dimensional (2D) materials, *e.g.* graphene oxide (GO),[2,3] MXene,[4] graphene nanosheets,[5,6] nanoflakes,[7] and layered double hydroxides,[8] into synthetic high-performance nanohybrids *via* covalent,[9–15] ionic[16–20] and/or supramolecular interactions.[21–35] As one of the most intensively studied 2D materials so far, GO nanosheets possess rich and tunable oxygenated functionalities on a surface that are accessible to engage *via* interfacial interactions with other materials ranging from polymers to metal ions;[16–20,24,33,34,36–47] and they hold huge potential in a variety of fields, such as water treatment,[48] smart devices,[49] and gas separation.[50]

In GO-based nanohybrids, an inherent trade-off of strength and toughness exists all along their development history as a crucial problem to be tackled. As crosslinkers, small organic compounds and multivalent metal ions are popular and can enhance the tensile strength and modulus of the resultant hybrid films, adversely at the price of compromised toughness, because these short and dense bridging units lack sufficient plastic deformation.[51] In view of this issue, polymers with linear chain conformation were introduced to crosslink the

[a] *Department of Materials and Environmental Chemistry, Stockholm University, Stockholm 10691, Sweden. E-mail: miao.zhang@mmk.su.se, jiayin.yuan@mmk.su.se*
[b] *Key Laboratory of Material Chemistry for Energy Conversion and Storage (Ministry of Education), School of Chemistry and Chemical Engineering, Huazhong University of Science and Technology, Luoyu Road No. 1037, Wuhan 430074, China*
[c] *Department of Chemistry & Department of Mechanical Engineering, Tsinghua University, Beijing 100084, China. E-mail: lqu@mail.tsinghua.edu.cn*

† Electronic supplementary information (ESI) available. See DOI: 10.1039/d1nh00073j

nanohybrids and meanwhile maintain and transfer their synergistic toughening effects to the nanohybrids to buffer the stretching force.[21,27,36–39,41,46] Lately, a macromolecular coupling concept termed "polycationitrile" has been introduced as an enabling tool to engineer polymer/inorganic interfaces,[52] where "polycationitrile" stands for a heterocyclic cation-methylene-nitrile functionality sequence that is coded into a polymer repeating unit. Such structural motifs are often seen in poly(ionic liquids) (PILs) and are also designable in general ionic polymers.[53–55] This macromolecular crosslinking tool is capable of cyclizing nitrile groups into triazine-based networks very efficiently under ambient conditions *via* a mild NH_3 vapor treatment.[56] We envision that the newly established polycationitrile concept is a game-changer to address abundant molecular or nanoscale interfaces, particularly in 2D hybrid materials.

In this contribution, the power of polycationitrile in engineering ultratough and ultrastrong 2D material-based hybrid films has been demonstrated. As exemplified with GO nanosheets, the tensile strength and toughness of the as-prepared GO-PIL hybrid films outperform the state-of-the-art GO-based hybrid films. As a distinctive advantage, the mechanical properties of our GO-PIL hybrid films have a fabulous tolerance against moisture as an added merit of this polymeric crosslinker.

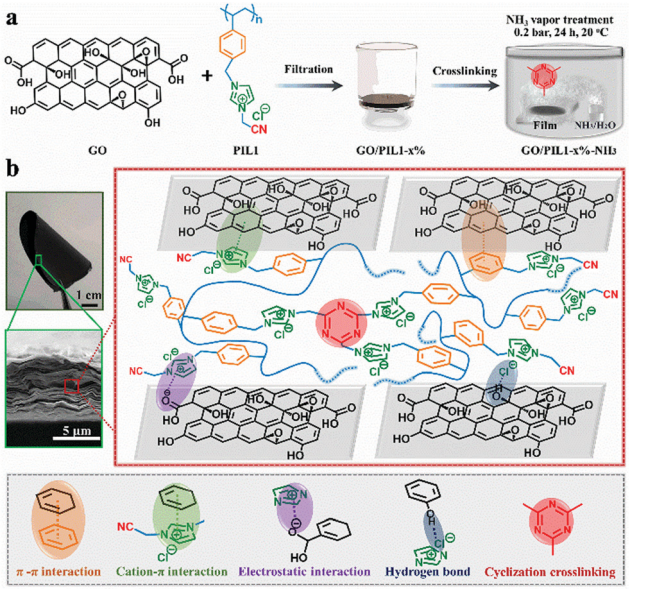

Fig. 1 (a) Schematic of the preparation procedure of the NH_3-treated GO/PIL1 hybrid films (GO/PIL1-***x***%-NH_3, ***x***% denotes the relative content of PIL1 to GO) *via* the polycationitrile approach. (b) The digital photograph of GO/PIL1-3%-NH_3, its cross-sectional SEM image, and the schematic of different types of covalent and non-covalent interactions in it.

Results and discussion

GO nanosheets employed in this study were synthesized at room temperature *via* the oxidation of natural graphite according to a modified Hummers' method.[57] The model polymer involved to assemble GO was poly(1-cyanomethyl-3-(4-vinylbenzyl) imidazolium chloride) (termed PIL1, chemical structure shown in Fig. 1a); its repeating unit carries the imidazolium-methylene-nitrile structural motif as the mandatory functionality sequence to operate the polycationitrile crosslinking reaction.[56] PIL1 was obtained *via* the radical polymerization of its ionic monomer (Fig. S1 and S2, ESI†). The preparation procedure of the GO/PIL1 hybrid film is schematically illustrated in Fig. 1a. In brief, two individual aqueous dispersions of GO and PIL1 were mixed upon sonication, and then their mixture dispersion was deposited into a film on a support *via* a pressure-assisted filtration method. The obtained film was annealed in NH_3 vapor (0.2 bar, 24 h, 20 °C) to crosslink PIL1, after which the target hybrid film was peeled-off easily from the support. Here, a series of the hybrid film samples with varied PIL1 contents were designed and termed as GO/PIL1-***x***%, where ***x***% denotes the relative amount of PIL1 to GO. The NH_3-treated films as the target product are termed GO/PIL1-***x***%-NH_3. Such hybrid films are mechanically flexible, and a representative cross-sectional scanning electron microscopy (SEM) image displays a typical laminated profile (Fig. 1b).

The covalent crosslinking reaction of polymer chains involves an NH_3-catalyzed room temperature cyclization reaction of the distal nitrile groups in PIL1 into a *s*-trizine-based network.[56] Besides this inter-chain covalent linkage, PIL1 also provides multiple synergistic non-covalent interfacial interactions with GO nanosheets. As suggested in Fig. 1b, the aromatic phenyl groups and the imidazolium cations of PIL1 interact with adjacent GO nanosheets *via* π–π, electrostatic and cation–π interactions. In addition, the counter anions (Cl^-) in PIL1 can build up hydrogen bonding with hydroxyl groups on GO nanosheets.[58] These multiple inter-/intra-molecular interactions engineered by PIL1 into the hybrids are crucial and join together to better the mechanical properties of nanohybrids, as discussed later.

The as-synthesized GO nanosheets were optimized and screened out the larger sized sheets with average area and thickeness of 10.33 ± 26.43 μm^2 and 0.75 ± 0.12 nm, respectively, as determined by SEM and atomic force microscopy (AFM) measurements (Fig. 2a and Fig. S3c, Table S1, ESI†), respectively. These GO nanosheets carry intrinsic wrinkles on their basal planes as a result of the sp^3-hybridized structural defects.[2,3,45,59] At the micron scale, GO/PIL1-3%-NH_3 is observed to be particularly rich in wrinkled textures (Fig. 2b and Fig. S4, ESI†), possessing *ca.* three times larger roughness (53 ± 12 nm in an area of 5 × 5 μm^2) than that of the pristine GO film (18 ± 2 nm, Fig. S5, ESI†). This is because intercalating PIL1 into laminated GO sheets could change the interlayer spacing and induce more disordered alignment during filtration and assembly, which was observed by the X-ray diffraction (XRD) analysis (Fig. 2c). A strong reflection peak in the range of 10°–12° was spotted in the XRD patterns of all samples, corresponding to the interlayer spacing. As expected, adding PIL1 stepwise into GO nanosheets shifts this diffraction peak towards smaller angles as a result of broadening of their interlayer spacing from 7.83 Å (for GO/PIL1-1%-NH_3) to 8.09 Å (for GO/PIL1-5%-NH_3) with respect to the pristine GO film (7.76 Å, Table S2, ESI†). In addition, the broader plateaus

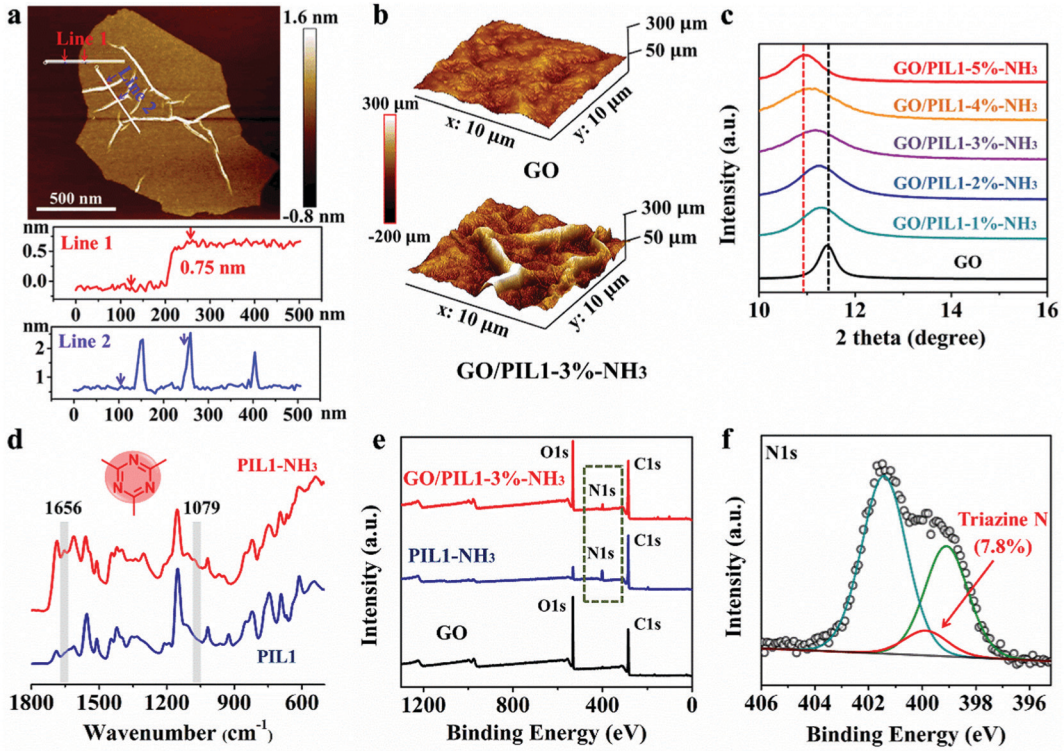

Fig. 2 (a) A representative AFM image of the as-prepared GO sheet and its corresponding height profile. (b) 3D AFM images of the pristine GO film (top) and GO/PIL1-3%-NH_3 (bottom). (c) XRD patterns of the pristine GO film and GO/PIL1-***x***%-NH_3, ***x*** = 1 to 5. (d) FT-IR spectra of PIL1 and its NH_3-treated sample PIL1-NH_3. (e) XPS spectra of the pristine GO film, PIL1-NH_3 and GO/PIL1-3%-NH_3. (f) The high resolution spectrum of N 1s of PIL1-NH_3.

were observed with the increasing content of PIL1 in the GO hybrid films, indicating a more disordered structure of these nanohybrids. Therefore, the PIL1 chains that are intercalated into adjacent GO nanosheets impact the layered microstructure, and in turn their mechanical properties, as discussed later.

Fourier transform infrared spectroscopy (FTIR) was performed to monitor the NH_3-triggered covalent crosslinking of PIL1. As shown in Fig. 2d, upon the NH_3 vapor treatment, two IR bands at 1656 cm^{-1} and 1079 cm^{-1} emerged with respect to the untreated state, which correspond to the ν(C=N) and ν(C–N) IR bands in the *s*-triazine rings, respectively.[60] In the X-ray photoelectron spectroscopy (XPS) tests, the pristine GO film displays two typical intense peaks at 287 (C 1s) and 532 eV (O 1s).[61] Both GO/PIL1-3%-NH_3 and NH_3-treated PIL1 (termed PIL1-NH_3) exhibit broad nitrogen signals around 400 eV (N 1s, Fig. 2e). Through peak deconvolution, the distinct N 1s peaks at 401.4 eV and 399.1 eV were identified, corresponding to the imidazolium N^+ and imidazolium N.[56] In addition, a peak at 399.9 eV is found and ascribed to the N species in the *s*-triazine rings (Fig. 2f), supporting the NH_3-catalyzed cyclization of the nitrile groups.[56,62]

The mechanical properties are the key goal of this study. The pristine GO film displays a tensile strength of 253 ± 16 MPa and a toughness of 5.19 ± 0.43 MJ m^{-3}, both of which are higher than those of conventional GO films prepared directly by the classic Hummers' method (tensile strength: 103 ± 20 MPa and toughness: 1.34 ± 0.52 MJ m^{-3}, Fig. S6a and Table S3, ESI†). This difference may stem from fewer structure defects and larger graphitic domains of our GO sheets that enable stronger inter-sheet interactions than that in conventional GO sheets prepared by the Hummers' method (Fig. S6b–e and Fig. S7, ESI†).[57] By depositing PIL1 chains into the GO film (even without NH_3 treatment), there appears immediately a mechanical improvement, *e.g.* the tensile strength and toughness of GO/PIL1-3% are 511 ± 43 MPa and 11.41 ± 1.01 MJ m^{-3}, respectively (Table S3, ESI†).

Upon NH_3 treatment, the inter-molecular crosslinking network of PIL1 *via* the cyclization of the nitrile groups further reinforces the interfacial interactions within GO nanohybrids. To note, the mechanical property of GO/PIL1-3%-NH_3 is a function of the exposure time towards NH_3 vapor (Fig. S8 and Table S4, ESI†). The tensile strength increases with the exposure time till 24 h, reaching a maximum of 585 ± 25 MPa, and so is same with the toughness of 14.93 ± 1.09 MJ m^{-3}, defining a modulus of 19.95 ± 2.60 GPa. These values are 2.3, 2.9 and 1.7 times those of the pristine GO film, respectively (Fig. 3a–c and Fig. S9, S10, ESI†). To stress, the tensile strength of GO/PIL1-3%-NH_3 is even as high as that of AISI 304 stainless steel,[2,63] but favorably with more flexibility and light weight. Care should be taken that although adding PIL1 to GO films is beneficial, overloading of PIL1 above 3 wt% weakens hybrid films mechanically. The detailed mechanical property data are listed in Table S3 (ESI†). The adverse overloading effect of PIL1 is obvious as excess PIL1 forms in the nanohybrids some bulk polymer micro-domains having less strength and toughness than GO, and such polymer micro-domains will deteriorate the

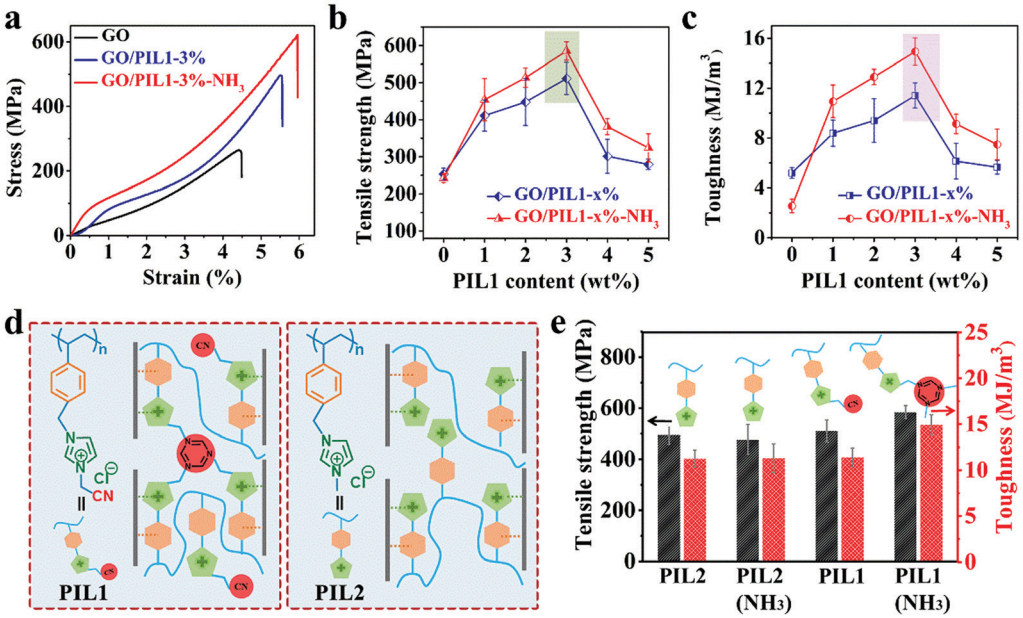

Fig. 3 (a) Tensile stress–strain plots of the pristine GO film (black), GO/PIL1-3% (blue), and GO/PIL1-3%-NH_3 (red). The comparisons of the tensile strength (b) and toughness (c) between GO/PIL1-***x***% (blue) and GO/PIL1-***x***%-NH_3 (red) with varied PIL1 contents, x = 0 to 5. When x = 0, GO/PIL1-0% is the pristine GO film and GO/PIL1-0%-NH_3 is the pristine GO film after the NH_3 treatment. (d) Schemes showing that PIL1 and a control polymer PIL2 were designed as crosslinkers into GO-based nanohybrids. (e) The tensile strength and toughness of hybrid films using different PILs (PIL1 and PIL2) before and after the NH_3 vapor treatment.

regular packing of GO nanosheets and cause a more disordered alignment (Fig. 2c). Besides, the pressure-assisted filtration method unavoidably forms some defects inside films with increasing thickness,[64] while there is negligible impact on the mechanical enhancement of the GO hybrid films caused by the polycationitrile crosslinking (Fig. S11 and Table S5, ESI†)

The polycationitrile effects of PIL1 on GO nanosheets can be elucidated by comparing the mechanical properties of nanohybrids prepared in a similar way *via* using a control polymer PIL2 (Fig. S12, ESI†). As shown in Fig. 3d, PIL2 holds a similar backbone to PIL1 but misses the distal nitrile group to undergo covalent crosslinking. As a proof, the NH_3 vapor treatment initiates the crosslinking of nitrile groups while little-to-no impact on nitrile-free PIL2, which was further confirmed by the FT-IR spectra of PIL2 and its NH_3-treated sample PIL2-NH_3 (Fig. S13, ESI†). As tested in Fig. 3e, the tensile strength and toughness of GO/PIL2-3%-NH_3 are 478 ± 58 MPa and 11.32 ± 1.56 MJ m^{-3}, respectively (Fig. S14 and Table S6, ESI†), which are higher than those of the pristine GO film but less than those of the GO/PIL1-3%-NH_3 sample. The detailed mechanical property data are listed in Tables S3 and S6 (ESI†). Fair to say, the nitrile group in PIL1 is crucial to the hybrids' mechanical properties *via* polycationitrile effects. In general, the observed superior mechanical properties of GO/PIL1-***x***%-NH_3 (***x*** = 1 to 5) systems are synergistically brought by (i) the nano-/microscale-layered packing of GO sheets that amplifies inter-GO interactions,[65] (ii) the multiple supramolecular interactions between PIL1 and GO sheets, and (iii) the covalent crosslinks of individual PIL1 chains that add extra merits. These three efforts add up together to the overall mechanical profile of the hybrid film.

Next, the stress–strain experiments under cyclic loading–unloading processes were conducted to reach an in-depth view of the key factors dictating their mechanical performance (Fig. 4a–c). In the initial stretching process, GO/PIL1-3%-NH_3 shows an elastic deformation within a strain of 0.5% reversible deformation (Fig. 4a), which stems naturally from the stretching and elongation of polymer chains along the force direction to buffer the stress. Upon further stretching, GO/PIL1-3%-NH_3 was elongated with a permanent deformation of 0.23% after five successive loading-unloading cycles within a strain of 1.0%, which exhibits a plastic characteristic, as shown in Fig. 4b. Continuous slippage occurs between adjacent GO nanosheets, followed by the breakage and partly rebuilding of supramolecular interactions between PIL1 chains and GO nanosheets to dissipate a large amount of energy. At an even higher strain of 5.0% (Fig. 4c), the permanent deformation increases to 0.58%, obtaining a high fracture strength at further increased force. Based on these analyses, a proposed fracture process of GO/PIL1-3%-NH_3 is presented in Fig. 4d. The polycationitrile crosslinks for absorbing energy could improve both the tensile strength and toughness. The fracture morphology of GO/PIL1-3%-NH_3 by SEM imaging in Fig. S15 (ESI†) visualizes, as we expected, the pulling-out of individual GO nanosheets caused by a high stretching force.

For the polymer-free pristine GO film, the NH_3 treatment decreases both tensile strength and toughness, as proven experimentally (Fig. S16a and Table S3, ESI†), although its modulus increases. This adverse effect ascribes presumably to two aspects: first, NH_3 can react with carboxylic acid groups on GO nanosheets and weaken hydrogen bonding between adjacent GO sheets. Second, NH_3 may react with the residue epoxy

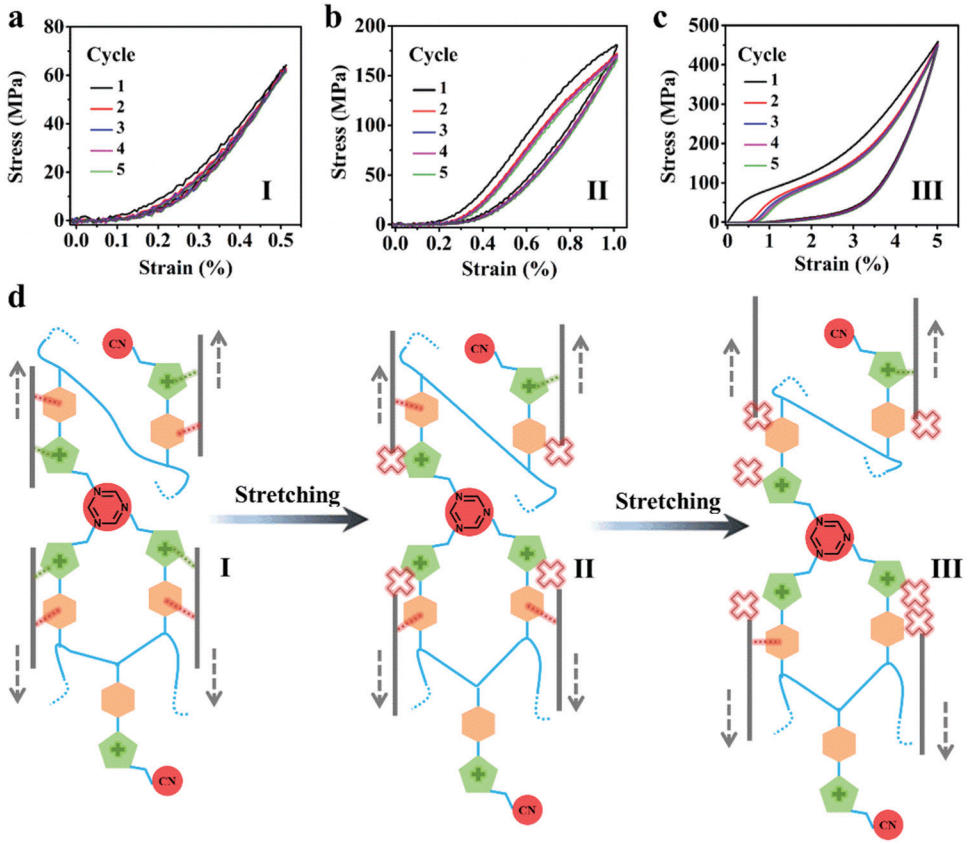

Fig. 4 Stress–strain curves of GO/PIL1-3%-NH_3 with strain of 0.5% (a), 1.0% (b) and 5.0% (c) under five successive loading–unloading cycles. (d) Schematic of the corresponding fracture process of GO/PIL1-3%-NH_3.

groups on GO nanosheets to slightly expand their interlayer spacing and construct rigid crosslinks between adjacent GO nanosheets (Fig. S16b–e, ESI†).[66] By contrast, NH_3-induced polycationitrile crosslinks endow GO-based hybrid films with integrated superior mechanical properties. To the best of our knowledge, in terms of strength and toughness, our GO/PIL1-3%-NH_3 sample is the best among GO-based nanohybrids ever reported (Fig. 5a and Table S7, ESI†).

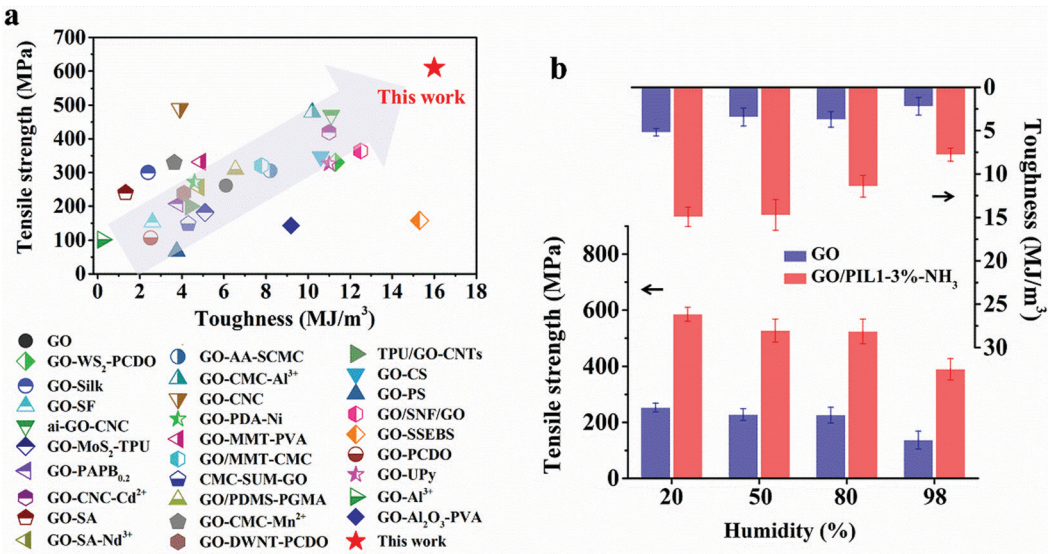

Fig. 5 (a) Comparison of the mechanical property of GO/PIL1-3%-NH_3 with a pure GO film and other GO-based nanohybrids known in literature. (b) The effects of environmental relative humidity on the mechanical properties of pure GO film and GO/PIL1-3%-NH_3. Tensile strength (bottom) and toughness (top).

The pristine GO film with oxygenated functional groups could bond between adjacent GO sheets directly *via* hydrogen bonds mediated by water molecules from moisture.[67,68] The gap between adjacent GO nanosheets would accommodate excessive water molecules at high RH, which could increase hydrogen bonding between water molecules but not bridge adjacent GO sheets. Not to forget, water as a Lewis base can nucleophilically attack GO with different oxygenation degrees, and weaken the plane-to-plane interaction, causing an unfavorable interlaminar swelling of GO sheets.[69] As a result, excessive moisture could swell the structure and facilitate lateral slippage of adjacent GO naonsheets, weakening the mechanical properties of GO and GO-based hybrid films.[70] The tensile strength, modulus and toughness of pure GO and GO/PIL1-3%-NH_3 films were found to gradually decrease with the increasing environmental RH from 20% to 98% (Fig. 5b and Fig. S17, ESI†). In this circumstance, GO/PIL1-3%-NH_3 can favorably maintain largely its tensile strength of 390 ± 38 MPa and toughness of 7.78 ± 0.75 MJ m^{-3} at an extreme RH of 98%, respectively, corresponding to almost 200% and 250% improvement in comparison to the pristine GO films at the same RH (137 ± 32 MPa, 2.19 ± 1.01 MJ m^{-3}, Table S8, ESI†). The significant retention of mechanical performance at RH = 98% in our opinion relies on the chemical stability of π–π stacking against moisture plus the covalent crosslinks in PIL1 that are more inert towards high RH. GO/PIL1-3%-NH_3 can keep its structure integrity after soaking in water for at least one week (Fig. S18, ESI†).

Conclusions

In summary, an ultratough and ultrastrong GO hybrid film was designed and produced *via* the polycationitrile strategy. Owing to the synergistic noncovalent and covalent interactions, such a film shows extraordinary mechanical performance, far beyond the pristine GO film. In particular, in terms of strength and toughness the tailor-made GO/PIL1-3%-NH_3 is the best among ever reported GO-based hybrid film. This superiority in mechanical performance has been further brought into the harsh condition, here at an extremely high RH of 98%, being the best in its kind at this RH. Such simple and novel design rationale enabled by interface engineering *via* the molecular crosslinking chemistry is expected to be generally applicable to other 2D materials; it will expedite and broaden the application spectrum of 2D hybrid films in the fields of aerospace, artificial muscles, energy harvesting, and more.

Conflicts of interest

There are no conflicts to declare.

Acknowledgements

J. Yuan is grateful for financial support from ERC Starting Grant NAPOLI-639720 from the European Research Council, Swedish Research Council Grant 2018-05351, Dozentenpreis 15126 from Verband der Chemischen Industrie e.V. (VCI) in Germany, the Wallenberg Academy Fellow program (Grant KAW 2017.0166) in Sweden, and the Stockholm Materials Hub *via* European Regional Development Fund (No. 20204027). L. Qu acknowledges the financial support from the Ministry of Science and Technology of China (2017YFB1104300), and NSFC-STINT (21911530143).

References

1 F. Barthelat, Z. Yin and M. J. Buehler, *Nat. Rev. Mater.*, 2016, **1**, 16007.
2 M. Zhang, Y. Wang, L. Huang, Z. Xu, C. Li and G. Shi, *Adv. Mater.*, 2015, **27**, 6708–6713.
3 J. Chen, Y. Zhang, M. Zhang, B. Yao, Y. Li, L. Huang, C. Li and G. Shi, *Chem. Sci.*, 2016, **7**, 1874–1881.
4 T. Zhou, C. Wu, Y. Wang, A. P. Tomsia, M. Li, E. Saiz, S. Fang, R. H. Baughman, L. Jiang and Q. Cheng, *Nat. Commun.*, 2020, **11**, 2077.
5 Y. Zhang, S. Gong, Q. Zhang, P. Ming, S. Wan, J. Peng, L. Jiang and Q. Cheng, *Chem. Soc. Rev.*, 2016, **45**, 2378–2395.
6 Q. Cheng, J. Duan, Q. Zhang and L. Jiang, *ACS Nano*, 2015, **9**, 2231–2234.
7 L. J. Bonderer, A. R. Studart and L. J. Gauckler, *Science*, 2008, **319**, 1069–1073.
8 H. B. Yao, H. Y. Fang, Z. H. Tan, L. H. Wu and S. H. Yu, *Angew. Chem., Int. Ed.*, 2010, **49**, 2140–2145.
9 Y. Gao, L.-Q. Liu, S.-Z. Zu, K. Peng, D. Zhou, B.-H. Han and Z. Zhang, *ACS Nano*, 2011, **5**, 2134–2141.
10 Y. Tian, Y. Cao, Y. Wang, W. Yang and J. Feng, *Adv. Mater.*, 2013, **25**, 2980–2983.
11 S. Park, D. A. Dikin, S. T. Nguyen and R. S. Ruoff, *J. Phys. Chem. C*, 2009, **113**, 15801–15804.
12 W. Cui, M. Li, J. Liu, B. Wang, C. Zhang, L. Jiang and Q. Cheng, *ACS Nano*, 2014, **8**, 9511–9517.
13 J. Y. Woo, J. H. Oh, S. Jo and C.-S. Han, *ACS Nano*, 2019, **13**, 4522–4529.
14 Q. Cheng, M. Wu, M. Li, L. Jiang and Z. Tang, *Angew. Chem., Int. Ed.*, 2013, **52**, 3750–3755.
15 A. Satti, P. Larpent and Y. Gun'ko, *Carbon*, 2010, **48**, 3376–3381.
16 S. Park, K.-S. Lee, G. Bozoklu, W. Cai, S. T. Nguyen and R. S. Ruoff, *ACS Nano*, 2008, **2**, 572–578.
17 C.-N. Yeh, K. Raidongia, J. Shao, Q.-H. Yang and J. Huang, *Nat. Chem.*, 2015, **7**, 166.
18 T. Gong, S. Won, J.-H. Kim, H.-J. Lee, C. Lee and S.-M. Lee, *Chem. Commun.*, 2015, **51**, 2671–2674.
19 R.-Y. Liu and A.-W. Xu, *RSC Adv.*, 2014, **4**, 40390–40395.
20 J.-Y. Kong, M.-C. Choi, G. Y. Kim, J. J. Park, M. Selvaraj, M. Han and C.-S. Ha, *Eur. Polym. J.*, 2012, **48**, 1394–1405.
21 S. Wan, Y. Li, J. Peng, H. Hu, Q. Cheng and L. Jiang, *ACS Nano*, 2015, **9**, 708–714.
22 X. Hu, S. Rajendran, Y. Yao, Z. Liu, K. Gopalsamy, L. Peng and C. Gao, *Nano Res.*, 2016, **9**, 735–744.
23 L. Zhang, Y. Zhang, F. Li, S. Yan, Z. Wang, L. Fan, G. Zhang and H. Li, *ACS Appl. Mater. Interfaces*, 2019, **11**, 12890–12897.

24 H. Zhao, Y. Yue, Y. Zhang, L. Li and L. Guo, *Adv. Mater.*, 2016, **28**, 2037–2042.
25 K. Shahzadi, X. Zhang, I. Mohsin, X. Ge, Y. Jiang, H. Peng, H. Liu, H. Li and X. Mu, *ACS Nano*, 2017, **11**, 5717–5725.
26 R. Xiong, K. Hu, A. M. Grant, R. Ma, W. Xu, C. Lu, X. Zhang and V. V. Tsukruk, *Adv. Mater.*, 2016, **28**, 1501–1509.
27 S. Wan, F. Xu, L. Jiang and Q. Cheng, *Adv. Funct. Mater.*, 2017, **27**, 1605636.
28 P. Ming, Z. Song, S. Gong, Y. Zhang, J. Duan, Q. Zhang, L. Jiang and Q. Cheng, *J. Mater. Chem. A*, 2015, **3**, 21194–21200.
29 P. Das, V. C. Mai and H. Duan, *ACS Appl. Polym. Mater.*, 2019, **1**, 1505–1513.
30 Y. Shu, T. You, B. Liang, H. Chen and P. Yin, *ACS Appl. Bio Mater.*, 2019, **2**, 5544–5550.
31 S. Gong, Q. Zhang, R. Wang, L. Jiang and Q. Cheng, *J. Mater. Chem. A*, 2017, **5**, 16386–16392.
32 S. Gong, W. Cui, Q. Zhang, A. Cao, L. Jiang and Q. Cheng, *ACS Nano*, 2015, **9**, 11568–11573.
33 Y. Li, Z. Xue, Y. Luan, L. Wang, D. Zhao, F. Xu, Y. Xiao, Z. Guo and Z. Wang, *Compos. Sci. Technol.*, 2019, **179**, 63–68.
34 S. Wan, J. Peng, Y. Li, H. Hu, L. Jiang and Q. Cheng, *ACS Nano*, 2015, **9**, 9830–9836.
35 S. Wan, Q. Zhang, X. Zhou, D. Li, B. Ji, L. Jiang and Q. Cheng, *ACS Nano*, 2017, **11**, 7074–7083.
36 K. W. Putz, O. C. Compton, M. J. Palmeri, S. T. Nguyen and L. C. Brinson, *Adv. Funct. Mater.*, 2010, **20**, 3322–3329.
37 Z. Tan, M. Zhang, C. Li, S. Yu and G. Shi, *ACS Appl. Mater. Interfaces*, 2015, **7**, 15010–15016.
38 J. Wang, J. Qiao, J. Wang, Y. Zhu and L. Jiang, *ACS Appl. Mater. Interfaces*, 2015, **7**, 9281–9286.
39 Y. Wang, T. Li, P. Ma, S. Zhang, H. Zhang, M. Du, Y. Xie, M. Chen, W. Dong and W. Ming, *ACS Nano*, 2018, **12**, 6228–6235.
40 Y. Wang, R. Ma, K. Hu, S. Kim, G. Fang, Z. Shao and V. V. Tsukruk, *ACS Appl. Mater. Interfaces*, 2016, **8**, 24962–24973.
41 S. Song, Y. Zhai and Y. Zhang, *ACS Appl. Mater. Interfaces*, 2016, **8**, 31264–31272.
42 L. Liu, Y. Gao, Q. Liu, J. Kuang, D. Zhou, S. Ju, B. Han and Z. Zhang, *Small*, 2013, **9**, 2466–2472.
43 S. Wan, H. Hu, J. Peng, Y. Li, Y. Fan, L. Jiang and Q. Cheng, *Nanoscale*, 2016, **8**, 5649–5656.
44 P. Song, Z. Xu, Y. Wu, Q. Cheng, Q. Guo and H. Wang, *Carbon*, 2017, **111**, 807–812.
45 M. Zhang, L. Huang, J. Chen, C. Li and G. Shi, *Adv. Mater.*, 2014, **26**, 7588–7592.
46 D. D. Kulkarni, I. Choi, S. S. Singamaneni and V. V. Tsukruk, *ACS Nano*, 2010, **4**, 4667–4676.
47 Y. Wen, M. Wu, M. Zhang, C. Li and G. Shi, *Adv. Mater.*, 2017, **29**, 1702831.
48 Y. Wei, Y. Zhang, X. Gao, Z. Ma, X. Wang and C. Gao, *Carbon*, 2018, **139**, 964–981.
49 X. Yu, H. Cheng, M. Zhang, Y. Zhao, L. Qu and G. Shi, *Nat. Rev. Mater.*, 2017, **2**, 17046.
50 Q. Xu, H. Xu, J. Chen, Y. Lv, C. Dong and T. S. Sreeprasad, *Inorg. Chem. Front.*, 2015, **2**, 417–424.
51 Z. An, O. C. Compton, K. W. Putz, L. C. Brinson and S. T. Nguyen, *Adv. Mater.*, 2011, **23**, 3842–3846.
52 K. Täuber, A. Dani and J. Yuan, *ACS Macro Lett.*, 2017, **6**, 1–5.
53 W. Zhang, Q. Zhao and J. Yuan, *Angew. Chem., Int. Ed.*, 2018, **57**, 6754–6773.
54 Y. Wang, Y. Shao, H. Wang and J. Yuan, *Acc. Mater. Res.*, 2020, **1**, 16–29.
55 K. Grygiel, J.-S. Lee, K. Sakaushi, M. Antonietti and J. Yuan, *ACS Macro Lett.*, 2015, **4**, 1312–1316.
56 Z. Dong, C. Zhang, P. Huawen, J. Gong, H. Wang, Q. Zhao and J. Yuan, *Mater. Horiz.*, 2020, **7**, 2683.
57 H. Chen, W. Du, J. Liu, L. Qu and C. Li, *Chem. Sci.*, 2019, **10**, 1244–1253.
58 B. Yin, X. Zhang, X. Zhang, J. Wang, Y. Wen, H. Jia, Q. Ji and L. Ding, *Polym. Adv. Technol.*, 2017, **28**, 293–302.
59 H. C. Schniepp, J.-L. Li, M. J. McAllister, H. Sai, M. Herrera-Alonso, D. H. Adamson, R. K. Prud'homme, R. Car, D. A. Saville and I. A. Aksay, *J. Phys. Chem. B*, 2006, **110**, 8535–8539.
60 M. J. Bojdys, J. O. Müller, M. Antonietti and A. Thomas, *Chem. – Eur. J.*, 2008, **14**, 8177–8182.
61 Z. Xue, P. Huang, T. Li, P. Qin, D. Xiao, M. Liu, P. Chen and Y. Wu, *Nanoscale*, 2017, **9**, 781–791.
62 T. T. Liu, R. Xu, J. D. Yi, J. Liang, X. S. Wang, P. C. Shi, Y. B. Huang and R. Cao, *ChemCatChem*, 2018, **10**, 2036–2040.
63 Y. Zhou, C. Chen, S. Zhu, C. Sui, C. Wang, Y. Kuang, U. Ray, D. Liu, A. Brozena, U. H. Leiste, N. Quispe, H. Guo, A. Vellore, H. A. Bruck, A. Martini, B. Foster, J. Lou, T. Li and L. Hu, *Mater. Today*, 2019, **30**, 17–25.
64 T. Gong, D. V. Lam, R. Liu, S. Won, Y. Hwangbo, S. Kwon, J. Kim, K. Sun, J. H. Kim and S. M. Lee, *Adv. Funct. Mater.*, 2015, **25**, 3756–3763.
65 S. Wan, J. Peng, L. Jiang and Q. Cheng, *Adv. Mater.*, 2016, **28**, 7862–7898.
66 M.-S. Park, S. Lee and Y.-S. Lee, *Carbon Lett.*, 2017, **21**, 1–7.
67 O. C. Compton, S. W. Cranford, K. W. Putz, Z. An, L. C. Brinson, M. J. Buehler and S. T. Nguyen, *ACS Nano*, 2012, **6**, 2008–2019.
68 X. Lin, X. Shen, Q. Zheng, N. Yousefi, L. Ye, Y.-W. Mai and J.-K. Kim, *ACS Nano*, 2012, **6**, 10708–10719.
69 C.-N. Yeh, K. Raidongia, J. Shao, Q.-H. Yang and J. Huang, *Nat. Chem.*, 2015, **7**, 166–170.
70 S. Wan, H. Hu, J. Peng, Y. Li, Y. Fan, L. Jiang and Q. Cheng, *Nanoscale*, 2016, **8**, 5649–5656.